Journal of Alloys and Compounds 693 (2017) 474–481

Contents lists available at ScienceDirect

Journal of Alloys and Compounds

journal homepage: http://www.elsevier.com/locate/jalcom

Structure and electrochemical performance of cobalt oxide layer coated on $LiNi_{0.03}Mn_{1.97}O_4$ cathode materials

Qingqing Wang [a], Yang Zhang [a], Huang Zhang [b], Yunlong Xu [a, *], Hui Dong [a], Chongjun Zhao [a]

[a] Key Laboratory for Ultrafine Materials of Ministry of Education, Shanghai Key Laboratory of Advanced Polymeric Materials, School of Materials Science and Engineering, East China University of Science and Technology, Shanghai 200237, PR China
[b] Helmholtz Institute Ulm, Helmholtzstrasse 11, D-89081 Ulm, Germany

ARTICLE INFO

Article history:
Received 24 May 2016
Received in revised form
9 August 2016
Accepted 12 September 2016
Available online 13 September 2016

Keywords:
$LiMn_2O_4$
Nickel doping
Cobalt oxide
Modification
Electrochemical performance

ABSTRACT

The composite cathode materials were fabricated by means of a thermal decomposition method combining a modified sol-gel method. The composite cathode-based cells exhibits improved electrochemical properties compared to the pristine lithium manganite cathode both at room temperature and boosted temperature. The cobalt oxide (Co_3O_4) characterized by the thermogravimetry play a protecting role from disproportionation manganese reaction and the considerable coating amount was 2% summarized from the electrochemical results. The cobalt oxide coating layer and the nickel doping ions showed a synergistic effect to ameliorate the electrochemical performance and the 2% coating combine with nickel doping cathode delivers the discharge capacity of 114.3 $mAhg^{-1}$ at current density of 148 mA/g with retention of 92.7% after 100th cycle as well as the rate capability. As what the results revealed that the cobalt oxide coating combined with nickel doping could be a considerable approach to improve the lithium manganate electrochemical properties and worth of further studies.

1. Introduction

Spinel $LiMn_2O_4$ undergoes severe capacity fading during long term charge-discharge cycles [1]. In order to mitigate above problems, various approaches have been attempted [2–4]. One of these approaches is to substitute Mn with transition metal elements into the bulk for the purpose to strengthen the crystal structure [5] and the other approach is modification by coating [6–8]. It has been addressed that Jahn–Teller distortions can be subdued by the substitution because of the decrease content of Mn^{3+}. There are many recent works on Ni doping modification and the obtained results showed that Ni doping could improve the electrochemical properties of $LiMn_2O_4$ [9–16]. Q. Wei showed that doping with Ni into the Mn sites can stabilize the structure and improve the cycling stability of $LiMn_2O_4$ [17]. H.M. Wu revealed that the Ni doped $LiNi_xMn_{2-x}O_4$ could increase the discharge capacities and improve the long cycle-life markedly [18]. Chen found that Ni, Mo co-doped can reduce Mn dissolution and significantly improved electrochemical performance of $LiMn_2O_4$ [19]. In spite of the finite improvement of cycle properties through doping the heterogeneous elements, $LiMn_2O_4$ still suffered from capacity attenuation owing to the disproportionation reaction of Mn dissolution stimulated by HF acid which is related to the electrolyte decomposition [20–23]. Therefore, surface coating modifications have been widely employed to prevent the interface contact so that inhibit the Mn dissolution reaction [24]. Many achieved studies showed that surface coating with various metal oxides such as Al_2O_3, SiO_2 and ZnO on the surface of cathode materials can efficiently improve their electrochemical properties [25,26]. Y. Shang reported that TiO_2 coating on the spinel surface can suppress the undesired SEI film and enhance the resistance of $LiMn_2O_4$ against hydrogen fluoride attack from the electrolytes [27]. Although there were plenty of reports aiming to improve the cycling stability of the $LiMn_2O_4$ materials, combination of doping and surface coating still remain in skimp and worth study.

Previous reports have shown that the Ni^{2+} doping can stabilize the structure, reducing Jahn–Teller distortions greatly, and metal oxide coatings can be taken to prevent the cathode from electrode/electrolyte interface undesired reaction, yielding an artificial protective layer. In the paper, we proposed the recombine doping Ni^{2+} into the bulk and surface coating modifications with Co_3O_4 and the

* Corresponding author.
E-mail address: xuyunlong@ecust.edu.cn (Y. Xu).

http://dx.doi.org/10.1016/j.jallcom.2016.09.130
0925-8388/

various contents of Co_3O_4-coated $LiNi_{0.03}Mn_{1.97}O_4$ were successfully synthesized via a thermal decomposition method. The effect of Co_3O_4 coating on $LiNi_{0.03}Mn_{1.97}O_4$ materials and their electrochemical properties were investigated and discussed systematically.

2. Experimental section

2.1. Synthesis of $LiNi_{0.03}Mn_{1.97}O_4$ materials

$LiNi_{0.03}Mn_{1.97}O_4$ materials were synthesized via a sol-gel method using citric acid (AR, Aldrich Chemical Co. Inc) as the chelating agent. Firstly, 0.5245 g lithium hydroxide monohydrate (AR, Aldrich Chemical Co. Inc) and 1.0507 g citric acid was added in deionized water at 50 °C. Then 0.0933 g Nickel (II) acetate tetrahydrate (AR, Aladdin Chemical Co. Ltd.) and 6.0353 g manganese (II) acetate tetrahydrate (AR, Aldrich Chemical Co. Inc.), molar ratio of 0.03:1.97, were dissolved and the solution was in 80 °C oil. The pH was adjusted to 7.5 by the addition of ammonium hydroxide (AR, Aldrich Chemical Co. Inc). The gel was totally dried and put into furnace pre-annealed at 350 °C for 4 h and then calcinated at 750 °C for 12 h under air atmosphere. The pure $LiMn_2O_4$ was synthesized under the same condition.

2.2. Synthesis of Co_3O_4 coating $LiNi_{0.03}Mn_{1.97}O_4$ materials

The Co_3O_4 coating $LiNi_{0.03}Mn_{1.97}O_4$ materials were synthesized by the following step: the mixture of as-prepared pristine $LiNi_{0.03}Mn_{1.97}O_4$ powders with cobalt (II) acetate tetrahydrate (AR, Aldrich Chemical Co. Inc) was in ethanol in ratios of (1.0 wt%, 2 wt%, 4.0 wt% the mass ratio of Co_3O_4 which is 1:99 ratio of Co_3O_4:$LiNi_{0.03}Mn_{1.97}O_4$). The mixture were ultrasonically agitated for 20 min and then mechanical stirred for 60 min subsequently, the mixture was dried at 80 °C followed by annealed at 400 °C for 3 h under air atmosphere and Co_3O_4-coated $LiNi_{0.03}Mn_{1.97}O_4$ materials were obtained after cooling to room temperature. The samples $LiMn_2O_4$ and $LiNi_{0.03}Mn_{1.97}O_4$ Co_3O_4-coated $LiNi_{0.03}Mn_{1.97}O_4$ (1.0 wt%, 2.0 wt%, 4.0 wt%) are marked as pristine LMO, N-0C-LMO, N-1C-LMO, N-2C-LMO and N-4C-LMO respectively.

2.3. Materials characterization

The crystallographic structure analysis was performed on powder X-ray diffraction (XRD, D/MAX, 2550V, Japan) with Cu-K_α radiation ($\lambda = 1.54056$ Å) and the obtained data was analyzed by software as well. $C_4H_6CoO_4 \cdot 4H_2O$ as the coating precursor was examined by a thermal gravimetric analysis (SDT Q600, Switzerland) with 10 °C min^{-1} of heating. The powder morphological feature characterization was carried out by field emission scanning electron microscopy (FESEM, Hitachi S-4800, Japan). Energy-dispersive spectroscopy that connected with SEM was applied to determine the elements content of the 2.0 wt% Co_3O_4-coated $LiNi_{0.03}Mn_{1.97}O_4$ sample and the Li elements cannot detected owing to the extremely small size. High-resolution transmission electron microscopy (TEM, JEM2010, JEOL) was carried out to observe the morphology feature of obtained samples.

2.4. Electrochemical tests

The electrochemical tests of the cathode material were investigated in button cell (2032 type) using Li metal as the anode. The cathode material powder, acetylene black (used as conduct material) and the binder polyvinylidene fluoride (PVDF) were homogeneous mixed in mass ratio of 80:10:10 in *N*-methyl-2-pyrrolidone (NMP) solvent to fabricate the working electrode. The mixture was then cast on aluminum foil and totally dried at 120 °C for 10 h under vacuum condition. The cathode loading is 1.7 mg/cm^2 and the assemble procedure of button cells were conducted in the argon-filled glove box with the separator (porous polypropylene film, Celgard 2320). The EC (ethylene carbonate) and DMC (dimethyl carbonate) were used as solvent (at 1:1 vol ratio) to dissolve 1 M $LiPF_6$ forming the electrolyte. The cells were placed to age for overnight to activation. Charge-discharge results were galvanostatically tested by the Land tester (CT2001A) between 3.0 and 4.4 V (vs. Li/Li^+) at 25 °C and 55 °C under the constant current density of 1C rate. The cyclic voltammetry (CV, 0.1 mV s^{-1}, 3.0–4.4 V) curves were obtained by the Electrochemical Workstation (CHI, 660B). The AC impedance spectra were proceeded at a frequency range of 10^5 Hz–10^{-2} Hz and the voltage bias is 3.0 V. The obtained AC impedance spectra were matched by the ZSim Demo software.

3. Results and discussion

3.1. Structure and morphology analyses

The XRD characterized the crystal structure of various synthesized pristine $LiMn_2O_4$ and Co_3O_4-coated $LiNi_{0.03}Mn_{1.97}O_4$ and the patterns were shown in Fig. 1. The diffraction peak corresponding 2θ of Si is used as the internal standard and the displacement error is 0.10°. It is observed from the patterns that no apparent changes of diffraction peak intense with the different coating amount of cobalt oxide layer on $LiNi_{0.03}Mn_{1.97}O_4$. All the sample patterns exhibit the same typical spinel phase of $LiMn_2O_4$ with the standard card (35-0782) in the Fd-3m symmetry and no peaks due to impurities were detected. The Rietveld refinement has been provided and the site occupancy of cations can described as $[Li]_{8a}[Mn_{1.97}Ni_{0.03}]_{16d}O_4$ and the 16 d location occupancy of cations is Mn 0.985, Co 0.000 Li 0.000, Ni 0.015 indicates that the Ni occupied in the16 d sites. The R_p is 7.14, R_{wp} 4.87, R_{exp} 5.51 respectively. This demonstrates that the Ni doping and cobalt oxide coating does not change the structures of $LiMn_2O_4$. The crystallite size of all the samples are all about 150 nm according to Scherrer formula $D = k\lambda/B\cos\theta$. In Table 1, the lattice parameter changes of the various samples were observed through the diffraction patterns using MDI Jade5.0 software. As seen from Table 1, the lattice parameter of crystallites of pure $LiMn_2O_4$ is 8.2465 Å while the Ni doped (sample N-0C-LMO) is 8.2410 Å resulting of the ions radius effect. Because Ni^{2+} ion substitute Mn^{3+} ions located in 16d sites and the introduction of Ni^{2+}

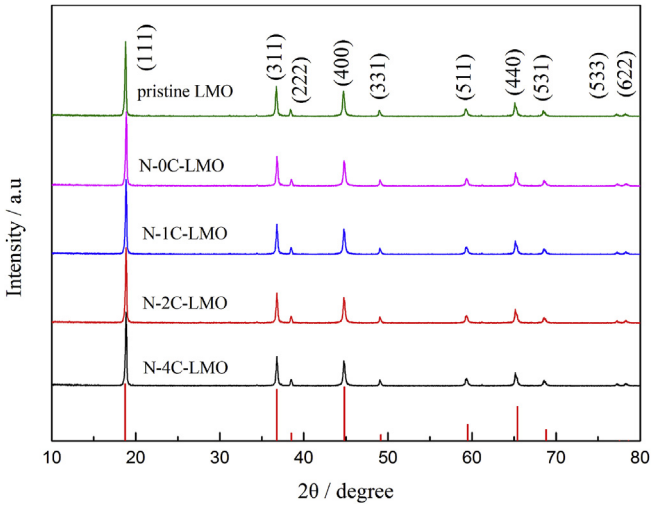

Fig. 1. XRD patterns of pristine $LiMn_2O_4$ and various Ni and Co_3O_4 coating samples.

Table 1
Crystal parameters of various synthesized samples.

Sample	a(Å)	Space group	Rwp (%)	Rp (%)
Pristine LMO	8.2465(2)	Fd3 m	7.48	5.14
N-0C-LMO	8.2410(2)	Fd3 m	6.47	4.01
N-1C-LMO	8.2404(3)	Fd3 m	6.38	3.98
N-2C-LMO	8.2409(4)	Fd3 m	7.14	4.87
N-4C-LMO	8.2406(2)	Fd3 m	8.44	6.17

can decrease the Mn^{3+} content on the contrary increasing the Mn^{4+} to maintain the valence balance, the shorter radius of Mn^{4+} than Mn^{3+} which the $R_{Mn3+} = 0.64$ Å, $R_{Mn4+} = 0.53$ Å, and $R_{Ni2+} = 0.69$ Å, CN = 6 as well [28–30], the lattice showed a shrinkage after the Ni doping. On the other hand, the ionic bond energy of Ni-O is higher than the Mn-O bond considering the decrease of Mn^{3+} which is closely related to the Jahn–Teller effect [31], the crystal structure stability was enhanced during the cycles [32]. It is observed that there is no obvious changes of the lattice parameters among the coating samples indicates that the Co_3O_4 would not turn into the cubic spinel structure.

Thermogravimetric measurement was carried out to confirm the chemical composition of the coating material $C_4H_6CoO_4 \cdot 4H_2O$ and the obtained curve were shown in Fig. 2. A drastic weight loss can be observed from 76 °C on account of the removal of water molecules in the sample and the value is 29.71%. The DTG curve calculation shows that another weight loss is appearing from 350 °C for the reason that the ongoing chemical reaction of phase transformation and the weight loss is 38.34%. The reactions are as follows [33]:

$$Co(CH_3COO)_2) \cdot 4H_2O \xrightarrow{\Delta} Co(CH_3COO)_2 + 4H_2O\uparrow \quad (1)$$

$$3Co(CH_3COO)_2 + \frac{25}{2}O_2 \xrightarrow{\Delta} Co_3O_4 + 12CO_2\uparrow + 9H_2O\uparrow \quad (2)$$

Hence, we selected 400 °C as the efficient temperature for the coating. The octahedral morphologies and element distribution of the Co_3O_4-coated $LiNi_{0.03}Mn_{1.97}O_4$ materials were observed through the SEM and EDS characterization. The observed SEM images of bare $LiMn_2O_4$ in Fig. 3(a), $LiNi_{0.03}Mn_{1.97}O_4$ in Fig. 3(b) and 2 wt% Co_3O_4-coated $LiNi_{0.03}Mn_{1.97}O_4$ samples in Fig. 3(c) are presented. As shown from the SEM images that the samples consist by particles with the size range of 200–300 nm and the surface of pristine $LiMn_2O_4$ shows a sharp surface, while the coated $LiNi_{0.03}Mn_{1.97}O_4$ samples display much coarser and rougher surface, indicating that surface of $LiNi_{0.03}Mn_{1.97}O_4$ has been successfully coated by Co_3O_4. The EDS analyses in the selected 2 wt% Co_3O_4 coated $LiNi_{0.03}Mn_{1.97}O_4$ sample region were performed so as to investigate the element distribution and the results are shown in Fig. 4. Fig 4(a) are the integral element distribution and Fig. 4(b) and (c) represent the mapping results of each individual elements of Mn, Ni, Co and O respectively. It can be distinctly observed from Fig. 4(b) that the Ni elements are in a homogeneous distribution meaning that the Ni doped in the crystal uniformly. Likewise, to further investigate the Co_3O_4 coating layer on the surface of cathode materials, the pure $LiMn_2O_4$ and 2 wt% Co_3O_4 coated $LiNi_{0.03}Mn_{1.97}O_4$ sample were analyzed via HR-TEM in Fig. 5(a) and (b). As can be seen in Fig. 5(a), no coating layer was observed on the pristine $LiMn_2O_4$ surface. The HR-TEM image in Fig. 5(a) and (b) indicates that the spinel $LiMn_2O_4$ is highly crystalline, and the lattice spacing of 0.47 nm are identical with that of the $LiMn_2O_4$ (111) plane. It can be seen clearly that Co_3O_4 coating forms over the $LiNi_{0.03}Mn_{1.97}O_4$ particles and the thickness of Co_3O_4 layer is about 6 nm which indicates that Co_3O_4 layer is successfully coated on the surface of the sample in Fig. 5(b) [34].

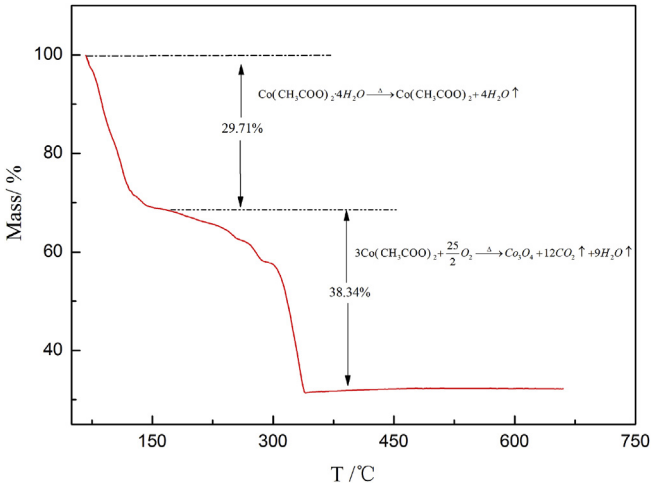

Fig. 2. TG curve of the coating medium $C_4H_6CoO_4 \cdot 4H_2O$.

The Brunauer-Emmett-Teller (BET) analyzer was performed to obtain the specific surface area and pore diameter distribution information of the Co_3O_4 coated $LiNi_{0.03}Mn_{1.97}O_4$ sample. Fig. 6 shows the curves of N_2 adsorption-desorption measured through the liquid nitrogen and the insert image is the obtained pore diameter distribution situation. As analysis result shown from Fig. 6 that the primary pore diameter is 3.74 nm meanwhile the obtained value of specific surface area is 1.93 $m^2\ g^{-1}$ and the volume of pores is 0.0071 $cm^3\ g^{-1}$ between 1.70 nm and 300.00 nm. The pore diameter and specific surface area were relatively lower versus to the other porous electrode materials [35,36]. The N_2 adsorption and desorption isotherms were belonged to the type II curve and a small hysteresis loop with a relative pressure (P/Po) between 0.1 and 0.9 can be seen from the curve implying that only few mesopores were existed in the structure of 2 wt% Co_3O_4 coated $LiNi_{0.03}Mn_{1.97}O_4$ sample [37]. The primary pore diameter is 3.67 nm and the specific surface area is 1.90 $m^2\ g^{-1}$ of the pristine $LiMn_2O_4$. the pore diameter and the specific surface area showed a tiny decrease after Co_3O_4 coating which may mainly due to the Co_3O_4 particle enter the $LiMn_2O_4$ pores partly, causing the slightly difference of the samples. The few pore structure was benefit for its compaction density meanwhile the lower specific surface area the less contact area between the Mn and electrolyte interface therefore dwindling the HF acid erosion, minimizing the tendency of Mn dissolution ultimately [38].

3.2. Electrochemical characteristics

The constant current charge-discharge test was performed to investigate the influence of Ni^{2+} and Co_3O_4 layer on the electrochemical characteristic of $LiMn_2O_4$ cathode material. Fig. 7 exhibits the first charge-discharge profiles of pristine and surface modified $LiNi_{0.03}Mn_{1.97}O_4$ samples at 0.5C between the potential of 3.0 V and 4.3 V (versus Li/Li^+) at 25 °C. From the plots in Fig. 7, the apparent discharge voltage plateaus were clearly observed from the charge-discharge curves of all the samples. The two potential regions were around 4.1 V and 3.9 V corresponding to the Li ions extraction from the active materials ($LiMn_2O_4 \rightarrow Li_{0.5}Mn_2O_4 + 0.5Li^+ + 0.5e^-$) and crystal phase transition ($Li_{0.5}Mn_2O_4 \rightarrow 2\lambda\text{-}MnO_2 + 0.5Li^+ + 0.5e^-$) which are in accordance with the discharge characteristic of the spinel $LiMn_2O_4$ [39,40]. The first discharge capacity of the pristine $LiMn_2O_4$ is 118.1 $mAhg^{-1}$, while those of sample $LiNi_{0.03}Mn_{1.97}O_4$, Co_3O_4-coated $LiNi_{0.03}Mn_{1.97}O_4$ (1.0 wt%, 2.0 wt%, 4.0 wt%) are 120.5,

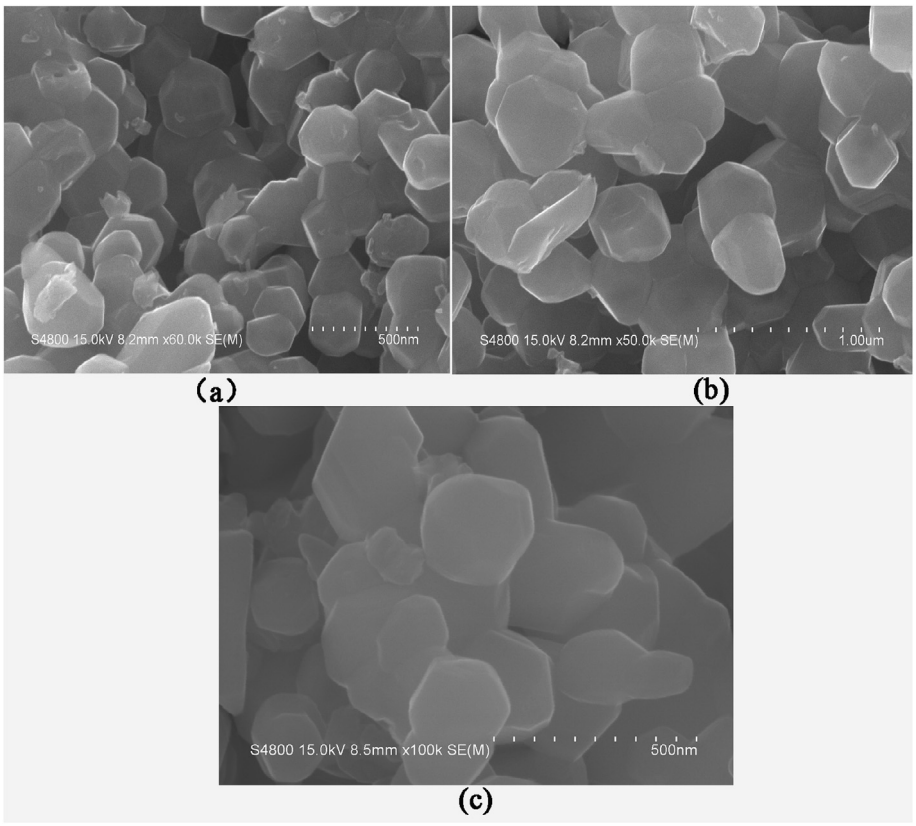

Fig. 3. SEM images of (a) pristine $LiMn_2O_4$, and (b) $LiNi_{0.03}Mn_{1.97}O_4$ and (c) 2 wt% Co_3O_4-coated $LiNi_{0.03}Mn_{1.97}O_4$.

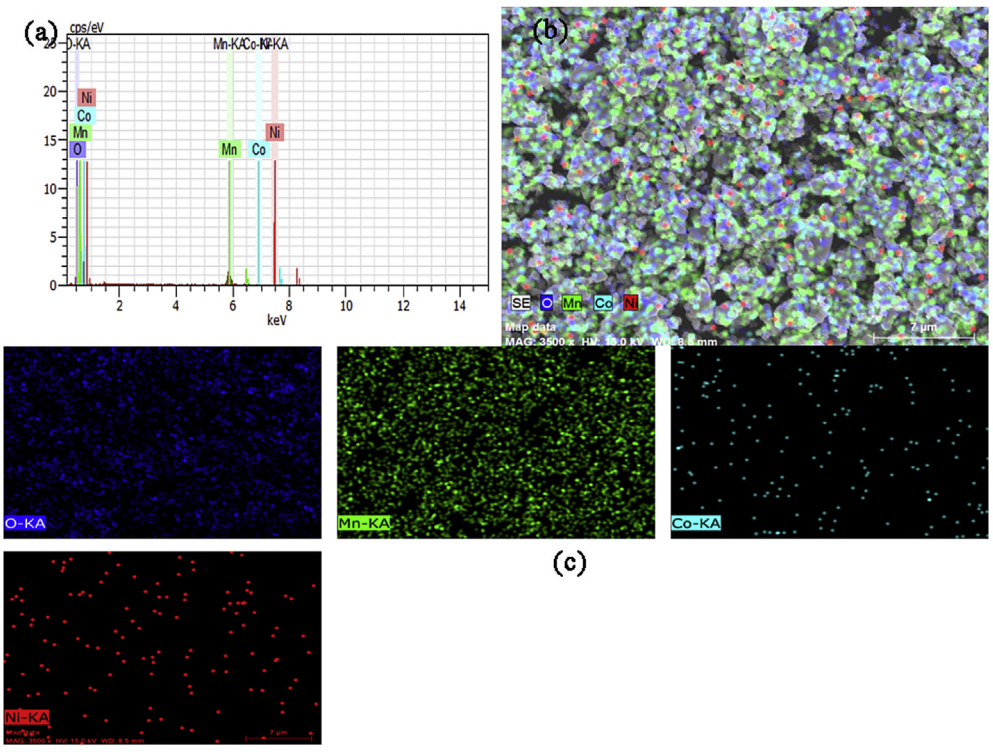

Fig. 4. EDS mapping result of the 2 wt% Co_3O_4-coated $LiNi_{0.03}Mn_{1.97}O_4$ sample.

122.0, 124.4, and 124.1 $mAhg^{-1}$, respectively. The discharge capacities of coated samples exhibit a slight higher than that of pristine one while the decrease of 4.0 wt% Co_3O_4-coated $LiNi_{0.03}Mn_{1.97}O_4$ sample may due to the nimiety of Co_3O_4 coating on

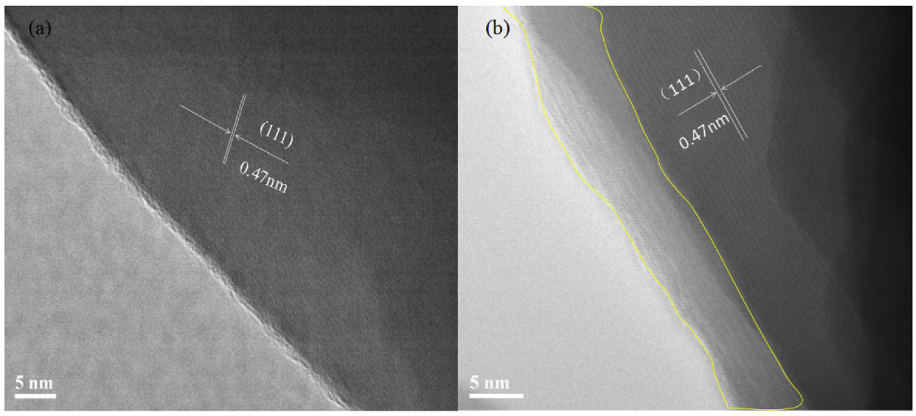

Fig. 5. TEM images of (a) pristine $LiMn_2O_4$ and (b) 2 wt% Co_3O_4-coated $LiNi_{0.03}Mn_{1.97}O_4$ sample.

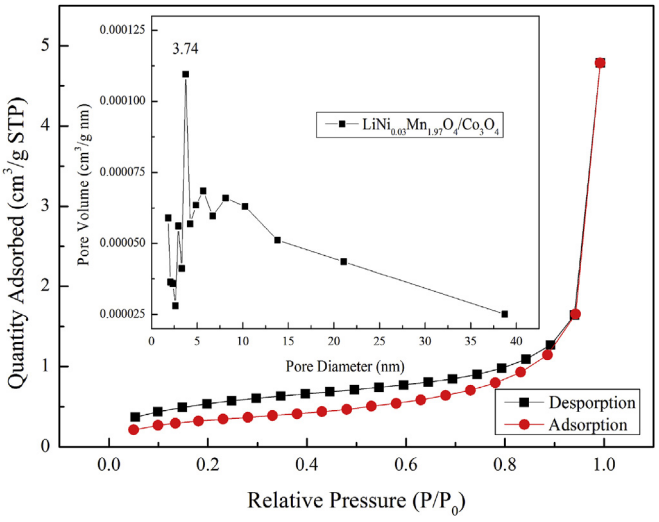

Fig. 6. N_2 sorption isotherms and pore size distributions of 2 wt% Co_3O_4-coated $LiNi_{0.03}Mn_{1.97}O_4$ sample.

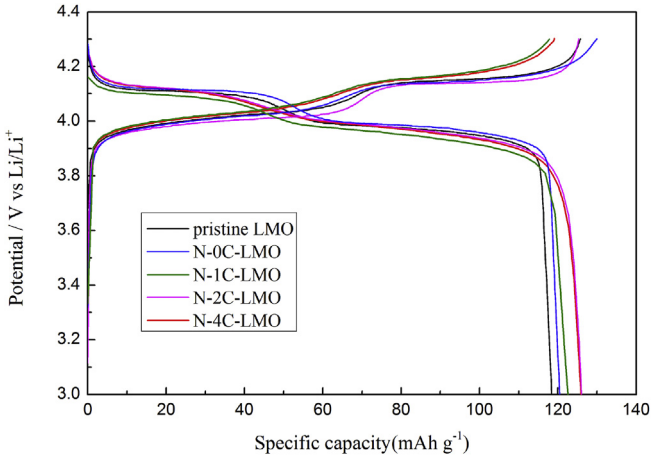

Fig. 7. Initial charge-discharge curves of various synthesized samples.

the active spinel $LiNi_{0.03}Mn_{1.97}O_4$.

The rate performances of all the samples were performed in the discharge current of 0.5C to the 10C top and finally recovered at 1 C again (five cycles at each rate) in Fig. 8. The samples revealed the

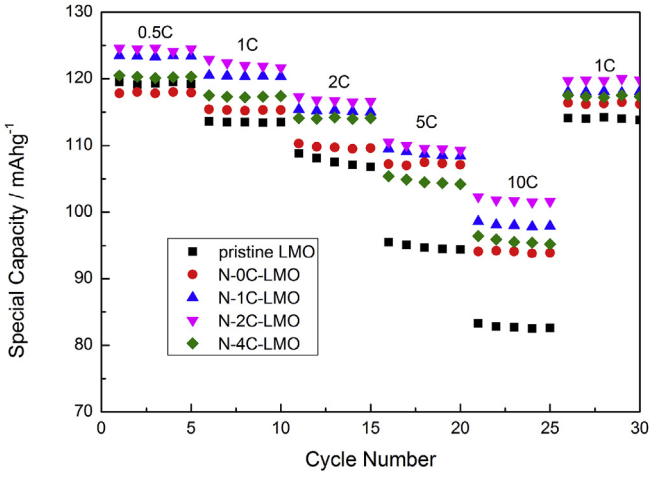

Fig. 8. Rate performances of various synthesized samples at room temperature (25 °C).

synchronous capacities fading with the augment of discharge rate which can be explained by the electron transport and Li^+ diffusion through the particles and the electrolyte interface which were the crucial process for the rate properties [41]. Significantly, the 2.0 wt% Co_3O_4-coated $LiNi_{0.03}Mn_{1.97}O_4$ sample delivered the preferable capacity in spite of any rates with superior rate stability than other samples may attributed to the reversible lithiation/delithiation under different rate as well as the effectively inhibited Mn dissolution from the inside $LiMn_2O_4$ electrode to the electrolyte, resulting in a lower Mn dissolution [42]. Because the good reversibility of Co_3O_4 coated sample but also the prevention of the direct contact between HF acid and the inner manganese from dissolving into the electrolyte, the 2.0 wt% Co_3O_4-coated $LiNi_{0.03}Mn_{1.97}O_4$ exhibited improved cycling stability [43]. The discharge capacities of 2.0 wt% Co_3O_4-coated $LiNi_{0.03}Mn_{1.97}O_4$ are 124.5 $mAhg^{-1}$ at 0.5C, 121.3 $mAhg^{-1}$ at 1C, 115.5 $mAhg^{-1}$ at 2C, 108.1 $mAhg^{-1}$ at 5C and 100 $mAhg^{-1}$ at 10C rates, respectively, which indicates that the 2.0 wt% Co_3O_4 coating is the most proper ratio to enhance the electrochemical properties of $LiMn_2O_4$.

The long-term cycling performances of all synthesized samples were carried out at room temperature (25 °C) at the charge-discharge current of 1C in Fig. 9. As shown in Fig. 9, the pristine $LiMn_2O_4$ only possesses the initial discharge capacity was 117.3 $mAhg^{-1}$ which decayed to 85.6 $mAhg^{-1}$ after 100 cycles remaining the 72.7% capacity approximately. Contrarily, the Co_3O_4 coated samples exhibited a certain improvement during the long-

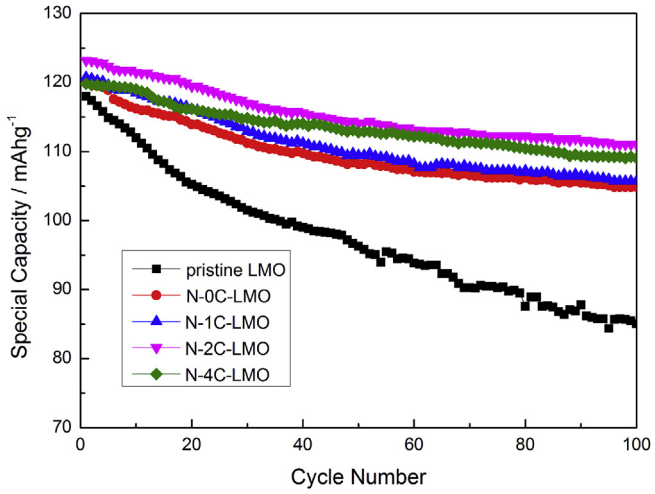

Fig. 9. Cyclic performances of various synthesized samples at rate of 1C at room temperature (25 °C).

cycle performances and the 2.0 wt% Co_3O_4-coated $LiNi_{0.03}Mn_{1.97}O_4$ sample showed the superior capability demonstrating that combine the dope and coating layer were able to improve the cycle stability of $LiMn_2O_4$ efficiently. The improved electrochemical performance mainly derived from two facts: (i) the more stable crystal structure by reason of the forming of partly intense Ni-O bond and the decrease of Mn^{3+} content which is beneficial for dwindling the Jahn-Teller distortion [9,17], (ii) Co_3O_4 layer effectively inhibiting the Mn dissolution from the $LiNi_{0.03}Mn_{1.97}O_4$ electrode into the electrolyte, resulting in a lower charge-transfer resistance [44–46]. In addition, it can be observed from the figure that the coating amount of 2.0 wt% Co_3O_4 coated sample exhibit the best cycling property however the cycling performance was deteriorating with the Co_3O_4 coating amount increases from 2.0 wt% up to 4.0 wt%. This manifests that there is an optimal amount of the Co_3O_4 layer content and once exceed the amount, it is adverse for improving the electrochemical performance.

Fig. 10 shows the cyclic performances of pristine $LiMn_2O_4$, $LiNi_{0.03}Mn_{1.97}O_4$ and 2 wt% Co_3O_4-coated $LiNi_{0.03}Mn_{1.97}O_4$ samples at the high temperature (55 °C) and discharge current of 1C. As expected, all samples especially pure $LiMn_2O_4$, showed capacity decay during the charge-discharge cycling which is mainly caused by the aggravated Jahn-Teller effect at high temperature [16]. The Initial capacities of the pristine $LiMn_2O_4$, $LiNi_{0.03}Mn_{1.97}O_4$ and 2 wt % Co_3O_4-coated $LiNi_{0.03}Mn_{1.97}O_4$ samples are 118.5 $mAhg^{-1}$ 118.7 $mAhg^{-1}$ 120.0 $mAhg^{-1}$ and the discharge capacity after 100th are 78.2 $mAhg^{-1}$ 92.4 $mAhg^{-1}$ 98.2 $mAhg^{-1}$ respectively. The capacity retention of all the samples is 66.3% 77.8% 81.8% respectively at a current density of 148 mA/g. It can be obviously seen that the specific capacity of pristine $LiMn_2O_4$ decreased more rapidly compared with other samples at elevated temperatures. The HF acid was generated more aggravate at high temperature because of the $LiPF_6$ decomposition which is related to the inevitable puny H_2O content. Relative references showed uniform coating layer can prevent Mn^{4+} ions from direct contact with the electrolyte and greatly decrease the capacity loss [47]. This result indicates the Ni doping and Co_3O_4 layer coating can significantly enhance stability the spinel structure and prevent the dissolution of Mn from the reaction with HF acid, contributing to the better electrochemical properties at high temperature.

The cyclic voltammograms of the pristine $LiMn_2O_4$, $LiNi_{0.03}Mn_{1.97}O_4$ and 2 wt% Co_3O_4-coated $LiNi_{0.03}Mn_{1.97}O_4$ cells are carried out in the voltage between 3.0 V and 4.4 V at the scan rate of 0.1 mV^{-1} after 100th discharge and the obtained curves were showed in Fig. 11. The CV curves of all the samples have two obvious redox peaks accorded with the intrinsic characteristic of the $LiMn_2O_4$. It can be seen from the CV curves that all the samples displayed apparent redox peaks and identical shapes of the curve, indicating that both the doping and coating would not change the inner redox potentials during the insert-extract process. The peak potential is slightly broadened increased, suggesting that the Co_3O_4-coated $LiNi_{0.03}Mn_{1.97}O_4$ sample has good reversibility and specific capacity. High intensity of peak currents ascribed to the improvement of the reversibility and electrochemical performances [17]. However, two pairs of anodic and cathodic peaks of 2 wt% Co_3O_4-coated $LiNi_{0.03}Mn_{1.97}O_4$ sample are much sharper and stable than other samples, which imply the effective improvement and the stabilization of the $LiMn_2O_4$ structure from the Ni doping and Co_3O_4 layer coating.

To further investigate the role of Ni doping and Co_3O_4 coating layer for $LiMn_2O_4$, the AC impedance spectroscopy was performed on the pristine $LiMn_2O_4$, $LiNi_{0.03}Mn_{1.97}O_4$ and 2 wt% Co_3O_4-coated $LiNi_{0.03}Mn_{1.97}O_4$ samples at a frequency range of 10^5 Hz–10^{-2} Hz. The electrochemical impedance spectroscopy of the samples and

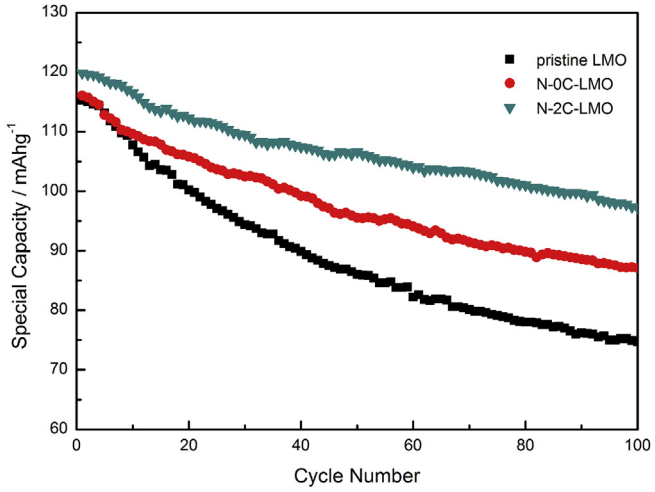

Fig. 10. Cyclic performances of pristine $LiMn_2O_4$, $LiNi_{0.03}Mn_{1.97}O_4$, 2 wt% Co_3O_4-coated $LiNi_{0.03}Mn_{1.97}O_4$ samples at rate of 1C at elevated temperature (55 °C).

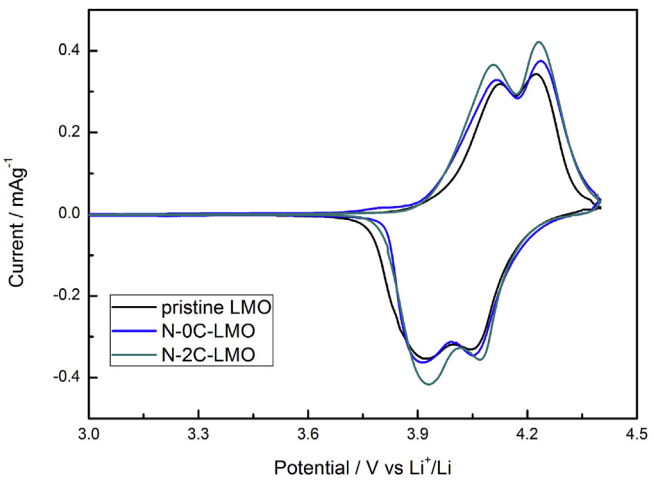

Fig. 11. CV curves of pristine $LiMn_2O_4$, $LiNi_{0.03}Mn_{1.97}O_4$, 2% Co_3O_4-coated $LiNi_{0.03}Mn_{1.97}O_4$ samples after 100th discharge.

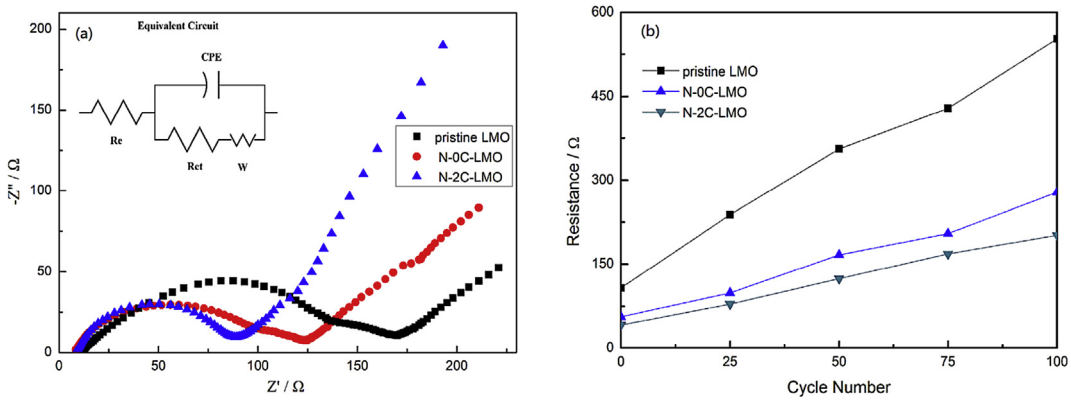

Fig. 12. (a) the Nyquist plots of pristine LMO, N-0C-LMO, and N-2C-LMO samples at first discharge and (b) the impedance changes with cycle and derived Rct at different cycles.

Table 2
The AC impedance analysis of various synthesized samples at first cycle.

Sample	R_e/Ω	R_{ct}/Ω	$W/\Omega\ cm^2\ s^{1/2}$
Pristine LMO	8.5	124.5	97.3
N-0C-LMO	20.7	67.5	78.9
N-2C-LMO	13.5	55.8	51.7

the insert equivalent circuit diagram are shown in Fig. 12. It can be identified that the impedance spectra were consisted of two parts, the semicircles part in the high-medium frequency and the linear part in low frequency. The semicircle represented the charge transfer resistance (R_{ct}) which is related to dual-effect of the interface between electrode and electrolyte and the (R_e) represented the electrolyte resistance meanwhile the linear part in low frequency region reflected the Warburg impedance (W) which is associated with the diffusion of Li ion in electrode [48]. The equivalent circuit parameters (R_e, R_{ct} and W) after the 50th cycle are also listed as shown in Table 2 for the samples severally. From the result of the 1st cycle, the Co_3O_4 coated $LiMn_2O_4$ exhibited slightly larger film resistance (R_f) than the bare $LiMn_2O_4$. This result can be attributed to the combination of the SEI film and Co_3O_4 coating layer formed on the surface of the Co_3O_4-coated electrode [49,42]. It was observed from Table 2 that a great reduction of Warburg impedance on $LiNi_{0.03}Mn_{1.97}O_4$ and 2.0 wt% Co_3O_4-coated $LiNi_{0.03}Mn_{1.97}O_4$ samples over pristine $LiMn_2O_4$ was for the reason of facilitates diffusion of Li^+ to electrode materials and the Warburg impedance inversely related to the Li^+ diffusion [45]. The 2.0 wt% Co_3O_4-coated $LiNi_{0.03}Mn_{1.97}O_4$ showed a lower charge transfer resistance (R_{ct}) value compared to pure $LiMn_2O_4$ from and there was an increase of (W) value of the pure $LiMn_2O_4$ more sharply than that of the 2.0 wt% Co_3O_4-coated $LiNi_{0.03}Mn_{1.97}O_4$ which changes from 55.8Ω to 166.4Ω with cycle in Fig. 12. The calculated resistances of 2 wt% Co_3O_4-coated $LiNi_{0.03}Mn_{1.97}O_4$ sample are the smallest in comparison with others, which indicates the Ni doping and Co_3O_4 coating can reduce the bulk resistance and the charge transfer resistance, improving their electrochemical kinetics and resulting in the enhanced high rate performance. Such results was well corroborated with the impedance growth rate and the impedance growth of pristine $LiMn_2O_4$ which was relatively faster than the doped-coating samples, indicating that Ni dope and Co_3O_4 coating layer would stable the crystal structure of $LiMn_2O_4$ material and decrease the dissolution of Mn^{4+} which leads to more admirable electrochemical performance. It can be seen that the AC impendence results were anastomotic with the above electrochemical test results of all the samples.

4. Conclusions

The Ni doping and Co_3O_4 coated spinel $LiMn_2O_4$ composites were successfully synthesized via a sol-gel combine with thermal decomposition method. can significantly improve the electrochemical performance of the $LiMn_2O_4$ materials. This highly crystalized and Co_3O_4 coated structure is beneficial to the compaction density and minimized the exposed area of the electrode to the electrolyte and thus decreased Mn^{2+} dissolution during the process. The 2.0 wt% Co_3O_4-coated $LiNi_{0.03}Mn_{1.97}O_4$ exhibited the good cycle performance both at room temperature and high temperature. As a universal sol-gel assisted synthesis method, it may also find application in the preparation of other coating layer materials. This convenient and successful strategy proposed in this study demonstrates a promising application in enhancing the performance of lithium manganite for lithium ion batteries.

Acknowledgements

The work is supported by Shanghai Nanotechnology Special Foundation (No. 11nm0500900), Shanghai Leading Academic Discipline Project (No. B502) and Shanghai Key Laboratory Project (No. 08DZ2230500).

References

[1] J. Lu, C. Zhan, T. Wu, J. Wen, Y. Lei, A.J. Kropf, H. Wu, D.J. Miller, J.W. Elam, Y.K. Sun, X. Qiu, K. Amine, Nat. Commun. 5 (2014) 5693.
[2] W. Wen, B. Ju, X. Wang, C. Wu, H. Shu, X. Yang, Electrochim. Acta 147 (2014) 271–278.
[3] X. Li, Y. Xu, C. Wang, J. Alloy. Compd. 479 (2009) 310–313.
[4] G. Amatucci, A.D. Pasquier, A. Blyr, T. Zheng, J.M. Tarascon, Electrochim. Acta 45 (1999) 255–271.
[5] Y. Wang, G. Yang, Z. Yang, L. Zhang, M. Fu, H. Long, Z. Li, Y. Huang, P. Lu, Electrochim. Acta 102 (2013) 416–422.
[6] T.-F. Yi, Y.-R. Zhu, X.-D. Zhu, J. Shu, C.-B. Yue, A.-N. Zhou, Ionics 15 (2009) 779–784.
[7] J.W. Fergus, J. Power Sources 195 (2010) 939–954.
[8] A. Mauger, C. Julien, Ionics 20 (2014) 751–787.
[9] A.A. Vereschaka, O.K. Hojaev, A.S. Vereschaka, I.S. Ruziev, Appl. Mech. Mater. 457–458 (2013) 120–126.
[10] M. Bakierska, M. Świętosławski, M. Gajewska, A. Kowalczyk, Z. Piwowarska, L. Chmielarz, R. Dziembaj, M. Molenda, Materials 9 (2016) 366.
[11] Y.C. Liu, M.C. Liu, R.L.H. Liu, M.C. Chi, Appl. Mech. Mater. 457–458 (2013) 93–97.
[12] F.X. Wang, S.Y. Xiao, Y. Shi, L.L. Liu, Y.S. Zhu, Y.P. Wu, J.Z. Wang, R. Holze, Electrochim. Acta 93 (2013) 301–306.
[13] Q. Wang, X. Zhang, Y. Xu, D. Liu, H. Dong, Y. Zhang, RSC Adv. 5 (2015) 75333–75340.
[14] P.K. Nayak, J. Grinblat, M. Levi, O. Haik, E. Levi, Y.-K. Sun, N. Munichandraiah, D. Aurbach, J. Mater. Chem. A 3 (2015) 14598–14608.
[15] B.J. Hwang, R. Santhanam, S.G. Hu, J. Power Sources 108 (2002) 250–255.
[16] D.-L. Fang, J.-C. Li, X. Liu, P.-F. Huang, T.-R. Xu, M.-C. Qian, C.-H. Zheng, J. Alloy. Compd. 640 (2015) 82–89.

[17] Q. Wei, X. Wang, X. Yang, B. Ju, B. Hu, H. Shu, W. Wen, M. Zhou, Y. Song, H. Wu, H. Hu, J. Mater. Chem. A 1 (2013) 4010.
[18] H.M. Wu, J.P. Tu, X.T. Chen, D.Q. Shi, X.B. Zhao, G.S. Cao, Electrochim. Acta 51 (2006) 4148–4152.
[19] M. Chen, P. Chen, F. Yang, H. Song, S. Liao, Electrochim. Acta 206 (2016) 356–365.
[20] C. Qing, Y. Bai, J. Yang, W. Zhang, Electrochim. Acta 56 (2011) 6612–6618.
[21] D. Aurbach, B. Markovsky, G. Salitra, E. Markevich, Y. Talyossef, M. Koltypin, L. Nazar, B. Ellis, D. Kovacheva, J. Power Sources 165 (2007) 491–499.
[22] Z. Yang, W. Yang, D.G. Evans, Y. Zhao, X. Wei, J. Power Sources 189 (2009) 1147–1153.
[23] D.H. Hu, S.X. Zhao, Y.F. Deng, C.W. Nan, J. Mater. Chem. 1 (2013) 14729–14735.
[24] G.H. Waller, P.D. Brooke, B.H. Rainwater, S.Y. Lai, R. Hu, Y. Ding, F.M. Alamgir, K.H. Sandhage, M.L. Liu, J. Power Sources 306 (2016) 162–170.
[25] J.S. Kim, C.S. Jahnson, J.T. Vaughey, S.A. Hackney, K.A. Walz, W.A. Zeltner, M.A. Anderson, M.M. Thackeray, J. Electrochem. Soc. 151 (2004) A1755–A1761.
[26] Y.K. Sun, K.J. Hong, J. Prakash, J. Electrochem. Soc. 150 (2002).
[27] Y. Shang, X. Lin, X. Lu, T. Huang, A. Yu, Electrochim. Acta 156 (2015) 121–126.
[28] S. Zhang, Y. Hu, J. Lumin. 177 (2016) 394–401.
[29] S. Güner, M. Amir, M. Geleri, M. Sertkol, A. Baykal, Ceram. Int. 41 (2015) 10915–10922.
[30] H. Yuan, X. Wang, Q. Wu, H. Shu, X. Yang, J. Alloy. Compd. 675 (2016) 187–194.
[31] O.K. Park, Y. Cho, S. Lee, H.C. Yoo, H.K. Song, J. Cho, Energy & Environ. Sci. 4 (2011) 1621–1633.
[32] G. Xu, Z. Liu, C. Zhang, G. Cui, L. Chen, J. Mater. Chem. A 3 (2015) 4092–4123.
[33] Y.Y. Yang, J.T. Sun, L.J. Yuan, K.L. Zhang, Wuhan Univ. J. 06 (2001) 660–662.
[34] C. Qing, Y. Bai, J. Yang, W. Zhang, Electrochim. Acta 56 (2011) 6612–6618.
[35] J. Deng, J. Pan, Q. Yao, Z. Wang, H. Zhou, G. Rao, J. Power Sources 278 (2015) 370–374.
[36] J.H. Lee, K.J. Kim, Electrochim. Acta 102 (2013) 196–201.
[37] Q.T. Qu, L.J. Fu, X.Y. Zhan, D. Samuelis, J. Maier, L. Li, S. Tian, Z.H. Li, Y.P. Wu, Energy Environ. Sci. 4 (2011) 3985–3990.
[38] X. Gao, Y. Sha, Q. Lin, R. Cai, M.O. Tade, Z. Shao, J. Power Sources 275 (2015) 38–44.
[39] J. Xie, K. Kohno, T. Matsumura, N. Imanishi, A. Hirano, Y. Takeda, O. Yamamoto, Electrochim. Acta 54 (2008) 376–381.
[40] D. Tonti, M.J. Torralvo, E. Enciso, I. Sobrados, J. Sanz, Chem. Mater. 20 (2008) 4783–4790.
[41] F. Jiao, J. Bao, A.H. Hill, P.G. Bruce, Angew. Chem. 47 (2008) 9711–9716.
[42] X. Zhang, Y. Xu, H. Zhang, C. Zhao, X. Qian, Electrochim. Acta 145 (2014) 201–208.
[43] Q. Chen, Y. Wang, T. Zhang, W. Yin, J. Yang, X. Wang, Electrochim. Acta 83 (2012) 65–72.
[44] K.Y. Chung, H.S. Lee, W.S. Yoon, J. Mcbreen, X.Q. Yang, J. Electrochem. Soc. 153 (2006).
[45] S. Zhao, Y. Bai, Q. Chang, Y. Yang, W. Zhang, Electrochim. Acta 108 (2013) 727–735.
[46] W.-K. Kim, D.-W. Han, W.-H. Ryu, S.-J. Lim, H.-S. Kwon, Electrochim. Acta 71 (2012) 17–21.
[47] D. Liu, Z. He, X. Liu, Mater. Lett. 61 (2007) 4703–4706.
[48] M. Prabu, M.V. Reddy, S. Selvasekarapandian, G.V. Subba Rao, B.V.R. Chowdari, Electrochim. Acta 88 (2013) 745–755.
[49] Y. Liu, W. Zhang, Y. Zhu, Y. Luo, Y. Xu, A. Brown, J.N. Culver, C.A. Lundgren, K. Xu, Y. Wang, Nano Lett. 13 (2013) 293–300.